CCD Photometry, Light Curve Deconvolution, Period Analysis, and Evolutionary Status of the HADS Variable V1116 Herculis

W. Allen Gilchrist, Jr.
Stonecrest Observatory, 104 Deer Ridge Drive, Fort Davis, TX 79734; gilchrist.allen@ymail.com

Kevin B. Alton
UnderOak and Desert Blooms Observatories, 70 Summit Avenue, Cedar Knolls, NJ; kbalton@optonline.net

Received June 9, 2023; revised September 15, 2023; accepted September 16, 2023

Abstract CCD-derived photometric B-, V-, R_c-, and I_c-magnitude data were acquired for V1116 Her, an intrinsic pulsating variable classified as a High Amplitude δ Scuti (HADS) star. Precise time-series light curve data were deconvolved using discrete Fourier transformation, revealing a fundamental mode (f_0) of oscillation at 10.5610 d^{-1} along with at least three other partial harmonics ($2f_0$—$4f_0$). At least nine other statistically significant frequencies were resolved following successive pre-whitening of each residual signal. An assessment of potential period changes over time was performed using 46 new times of maximum (ToMx) light produced from the present study (2022) along with 160 other ToMx values extracted from the TESS survey earlier in 2022. These results indicate that no substantive change in the fundamental period of oscillation or amplitude (nominally I_c-mag) has likely occurred over the past two years. Finally, an investigation with PARSEC models for generating stellar tracks and isochrones provided a better understanding about the evolutionary status of this star.

1. Introduction

V1116 Herculis (GSC 1510-1091) is a pulsating variable classified as a High Amplitude δ Scuti (HADS) star. The star was listed as a short period variable designated as 61.1935 Her in the article 162 Neue Veränderliche (Hoffmeister 1935). This variable was included in "The All Sky Automated Survey. Catalog of Variable Stars. I. 0 h–6 h Quarter of the Southern Hemisphere" (Pojmaṇski 2002), and was classified as either a δ Sct or β Cep star. V1116 Her was also imaged during the Robotic Optical Transient Search Experiment (ROTSE-I) survey (Woźniak, *et al.* 2004). Khruslov (2006) identified the star as a δ Sct pulsating variable. The "79th Name-List of Variable Stars" (Kazarovets *et al.* 2008) also lists the object as a δ Sct (DSCT) star with the name V1116 Her. Mining "The All-Sky Automated Survey for Supernovae (ASAS-SN) Light Curve Server v1.0" also uncovered a light curve for this intrinsic variable (Kochanek *et al.* 2017).

Less than 1% of δ Sct variables are HADS stars (Lee *et al.* 2008), but they are interesting targets for amateur photometrists with CCD or CMOS cameras installed on modestly-sized telescopes. With their relatively short pulsation periods (< 0.2 d), high variation amplitude (> 0.2 mag), and luminosity (> 10 $L_\odot$), it is possible to acquire a complete light curve (LC) in just a few observing sessions. Common among A- through F-type variable stars are the periodic or multi-periodic δ Scuti-type (hereafter δ Sct) pulsating stars. Such stars occupy a small space at the intersection of the classical instability strip, the pre-main sequence, and the main sequence (MS) on the Hertzsprung-Russell diagram. Observationally as a group, they represent the middle ground between high-amplitude radial pulsators, like Cepheid variables, and non-radial multi-periodic pulsators (Breger 2000). Main sequence δ Sct stars typically have spectral types between F2 and A2 (Rodríguez and Breger 2001) with temperatures ranging from 6300 to 8600 K (Uytterhoeven *et al.* 2011). Generally, hotter δ Sct stars have shorter pulsation periods (i.e. higher pulsation mode frequencies) than cooler ones.

Pulsations in δ Sct stars are generated by the kappa-mechanism operating in a He II partial ionization zone (T ~ 50000 K). Variations in levels of ionization and transparency in these zones cause low-order pressure (p) modes similar to acoustic waves (Cox 1963; Chevalier 1971). These can produce either radial pulsations evoking symmetrical changes in stellar size or non-radial pulsations giving rise to asymmetric changes in shape but not volume, or a combination of both radial and non-radial components. Although shorter periods (< 30 min) have been observed (Holdsworth *et al.* 2014) in some A-type stars, the fundamental mode radial pulsations of Galactic δ Sct variables with near solar metallicity are generally between 0.05 and 0.25 d. Masses range from ~ 1.2 $M_\odot$ to 2.5 $M_\odot$, so they are more luminous and larger than our Sun.

Stars with slower rotational velocities (< 30 $Km \cdot s^{-1}$) tend to be radial pulsators with light curve amplitudes (V-mag) in excess of 0.20–0.30 mag. These stars belong to a δ Sct subgroup called HADS variables.

HADS variables usually oscillate with low-order single or double radial pulsation modes (Poretti 2003a, 2003b; Niu *et al.* 2013, 2017). About 40% of HADS variables are double pulsators with simultaneous pulsations in the fundamental mode and the first overtone mode with amplitudes generally higher in the fundamental mode (McNamara 2000). HADS stars have historically been divided corresponding to their metallicity relative to our Sun ([Fe/H] = 0 dex). Stars in the metal-poor ([Fe/H] << 0) group are called SX Phe stars, based on the prototype SX Phoenicis.

A large number of HADS stars have been detected with precise photometry using much more sensitive space telescopes like the European Space Agency's CoRoT (Baglin 2003), the Canadian Microvariability and Oscillations of STars (MOST)

(Walker *et al.* 2003), NASA's Kepler (Gilliland *et al.* 2010; Guzik 2021; Yang *et al.* 2021), and the Transiting Exoplanet Survey Satellite (TESS) (Ricker *et al.* 2015; Bedding *et al.* 2020).

Pulsating stars have served as standard candles for determining celestial distances ever since Henrietta Leavitt discovered a period-luminosity (P-L) relationship of 25 Cepheid variables in the Small Magellanic Cloud (Leavitt and Pickering 1912). This P-L relationship has been improved over time based on differences between metal-rich (Population I) and metal-poor (Population II) Cepheids (Baade 1956). Ziaali *et al.* (2019) reported a refinement of the P-L relationship for δ Sct variables based on the more accurate values from the Gaia Mission (Lindegren *et al.* 2016; Gaia Collab. *et al.* 2018). A more recent investigation by Poro *et al.* (2021) resulted in another derivation of P-L relationships for δ Sct stars oscillating in the fundamental mode (adopted herein) as well as first through third overtones.

2. Observations, data reduction, and photometric processing

2.1. Photometry

Precisely timed photometric observations were made from the Stonecrest Observatory (SO) near Fort Davis, Texas (103.9767 W, 30.6167 N), with an SBIG ST10-XME CCD camera at the secondary focus of a 0.3-m f/8 Ritchey-Chretien telescope. This instrument produces a field of view (FOV) of 21' × 14' with an image scale of 1.73 arcsec/pixel (bin = 3 × 3). This binning produces images with adequate resolution compared to the typical seeing during summer in the mountains of west Texas. SO data used in this study were taken between July 12 and September 5, 2022. Images were acquired using TheSkyX Pro Version 10.5.0 (Software Bisque 2019) which controlled an Astro-Physics AP-1200 GTO German equatorial mount. The CCD-camera was equipped with B, V, R_c, and I_c filters manufactured to match the Johnson-Cousins Bessell specification. Dark subtraction, flat correction, and registration of all images collected at SO were performed with ImagesPlus Ver. 6.5 (ImagesPlus 2020). A few images were registered using AIP4Win V. 2.4.0 (Berry and Burnell 2005). These programs were also used to determine FWHM or HFD values to aid in aperture selection for photometric analysis. Exposures varied somewhat during the observations depending on sky conditions. Instrumental readings were reduced to catalog-based magnitudes using the APASS star fields (Henden *et al.* 2009, 2010, 2011; Smith *et al.* 2011) built into MPO Canopus v10.8.5.0 (Minor Planet Observer 2010). LCs were generated using ensembles of five non-varying comparison stars. The identities, J2000 coordinates, APASS V-magnitudes, and color indices (B–V) for V1116 Her and the comparison stars are provided in Table 1; a corresponding image showing the target and comparison stars is presented in Figure 1. Only data from images taken above 30° altitude (airmass < 2) were included; considering the proximity of all program stars, differential atmospheric extinction was ignored. The average uncertainty in the target star magnitudes for all four filters was less than 0.007, and in no case was the uncertainty greater than 0.014 mag. All photometric data acquired and used in this study can be retrieved from the AAVSO International Database (Kafka 2021; observer code GWAA).

Table 1. Astrometric coordinates (J2000), V-mag and color indices (B–V) for V1116 Her and five comparison stars (1–5) used during this photometric study.

	FOV ID	*R.A. (J2000) h m s*	*Dec. (J2000) ° ′ ″*	*APASS[a] V mag*	*APASS[a] (B–V)*
T	V1116 Her	16 30 16.40	+16 55 06.0	11.284	0.291
1	GSC 1510-1179	16 30 39.02	+16 59 24.1	12.477	0.751
2	GSC 1510-1221	16 30 33.78	+17 02 40.7	12.417	0.673
3	GSC 1510-1191	16 30 27.43	+17 00 30.8	12.757	0.543
4	GSC 1510-1134	16 29 52.73	+16 57 42.0	12.556	0.542
5	GSC 1510-1104	16 30 56.29	+16 54 48.9	12.743	1.18

[a] *V-mag and (B–V) for comparison stars derived from APASS database described by Henden* et al. *(2009, 2010, 2011) and Smith* et al. *(2011), as well as on the AAVSO web site (http://www.aavso.org/apass).*

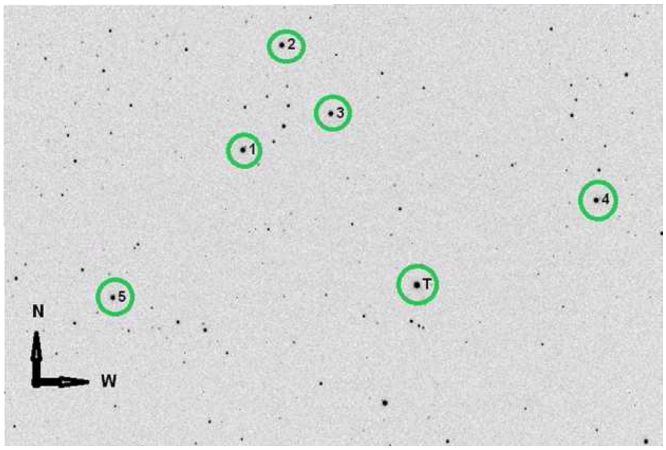

Figure 1. V1116 Her (T) along with the five comparison stars (1–5) used to reduce time-series images to APASS-catalog based magnitudes.

3. Results and discussion

3.1. Photometry and ephemerides

A total of 1247 measurements (316 B, 314 V, 309 R_c, and 308 I_c) were acquired between July 15 and September 5, 2022 (JD2459775.42014–2459827.48472). Figure 2 shows folded LCs for each filter produced with MPO Canopus. Period determinations were initially performed using Peranso v2.5 (Paunzen and Vanmunster 2016) by applying periodic orthogonals (Schwarzenberg-Czerny 1996) to fit observations and analysis of variance (ANOVA) to assess fit quality. Period solutions for different passbands can be slightly different. In this case, values of 0.094697 ± 0.00006 d were found for the B filter, with 0.094667 ± 0.00003 d for the V, R_c, and I_c filters. We also found 10,876 time-series values taken (cadence = 120 s) by the Transiting Exoplanet Survey Satellite (TESS) (Ricker *et al.* 2015; Bedding *et al.* 2020). These data (18 May 2022–13 June 2022) are available through the Mikulski Archive for Space Telescopes (mast.stsci.edu). Processing (ANOVA) these values (BJD_TDB vs. PDCSAP_FLUX) through Peranso 3 produced a folded light curve (Figure 3) with a period of 0.0946783 ± 0.0000093 d.

Another way to historically evaluate the period of oscillation is to compare the measured times of maximum light (ToMx) with those predicted by a reference ephemeris. An updated ephemeris can be determined by adjusting the parameters to

achieve the best fit to a plot of predicted time differences (PTD) versus cycle number. One advantage of this type of analysis is that data from different sources can be easily combined. In this case, for example, the star brightness in the TESS data is presented as normalized flux while the SO values are magnitudes estimated from APASS standards. The TESS data yielded 160 ToMx results, while a total of 46 new ToMx values were estimated from the SO data. The polynomial extremum fit utility in PERANSO 2.5 (Paunzen and Vanmunster 2016) was used for all ToMx determinations. No obvious color dependencies were seen in the SO timings. Table 2 contains a representative sampling of data acquired from TESS and SO. A complete set of 206 ToMx values from TESS and SO are available in a table found at:

ftp://ftp.aavso.org/public/datasets/3893-Gilchrist-V1116 Her.xlsx

and

ftp://ftp.aavso.org/public/datasets/3893-Gilchrist-V1116 Her..csv.

While determining ToMx times from the TESS data, it was clear that the amplitude of the variation and the mean brightness for V1116 Her are not constant. This will be discussed more fully in the section on Fourier analysis. The AAVSO International Variable Star Index (VSX; Kafka 2021) reference epoch (August 08, 2020) was initially defined by the following linear ephemeris (Equation 1):

$$\text{Max (HJD)} = 2459070.222 + 0.09468113\ E. \qquad (1)$$

Table 2. Differences between the times-of-maximum light (HJD) predicted from the updated linear ephemeris (Equation 2) and those observed for V1116 Her by the TESS satellite (18 May 2022–13 June 2022) and at Stonecrest Observatory (12 July 2022 and 05 Sept 2022). Sample table (see note).

Source	*Bandpass*	*ToMx HJD = 2400000+*	*ToMx Uncertainty*	*Cycle No.*	*PTD[a]*
TESS	I_c[b]	59718.70104	0.00115	–1151	0.00161
TESS	I_c	59718.79370	0.00128	–1150	–0.00041
TESS	I_c	59718.88866	0.00131	–1149	–0.00012
TESS	I_c	59718.98245	0.00120	–1148	–0.00101
TESS	I_c	59719.07954	0.00107	–1147	0.00139
TESS	I_c	59719.17131	0.00130	–1146	–0.00151
TESS	I_c	59719.26726	0.00118	–1145	–0.00023
TESS	I_c	59719.36418	0.00117	–1144	0.00200
SO	V	59772.66405	0.00130	–581	–0.00189
SO	R_c	59772.66462	0.00104	–581	–0.00132
SO	I_c	59772.66575	0.00155	–581	–0.00018
SO	B	59772.66620	0.00212	–581	0.00026
SO	I_c	59804.66630	0.00172	–243	–0.00083
SO	R_c	59827.67087	0.00118	0	–0.00303
SO	B	59827.67655	0.00184	0	0.00265
SO	V	59827.67760	0.00002	0	0.00370

[a] *(PTD) = Time difference between observed fundamental mode pulsation time-of-maximum and that calculated using the reference ephemeris (Equation 2).*
[b] *(I_c) = Bandpass for TESS satellite detector is between 600 and 1000 nm, centered near Cousins I. Note: Only the first eight values from TESS and the last eight from SO are shown in this sample table. Full table available at: ftp://ftp.aavso.org/public/datasets/3893-Gilchrist-V1116 Her.xlsx and .csv.*

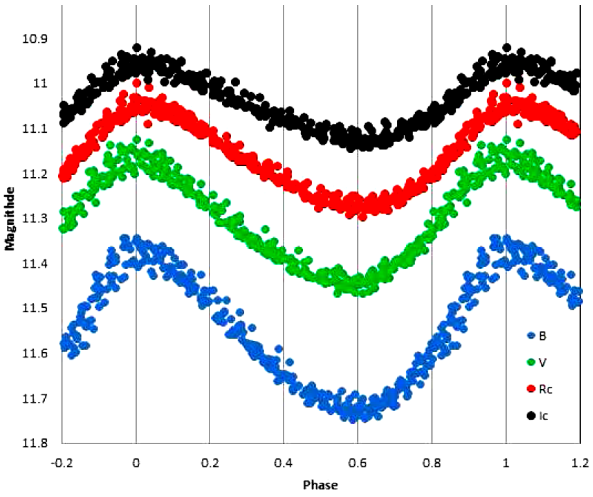

Figure 2. Period-folded (0.0946781 d) LCs for V1116 Her produced from photometric data obtained between July 15 and September 5, 2022, at SO. LCs shown top to the bottom are I_c, R_c, V, and B passbands and represent catalog-based (APASS) magnitudes determined using MPO CANOPUS.

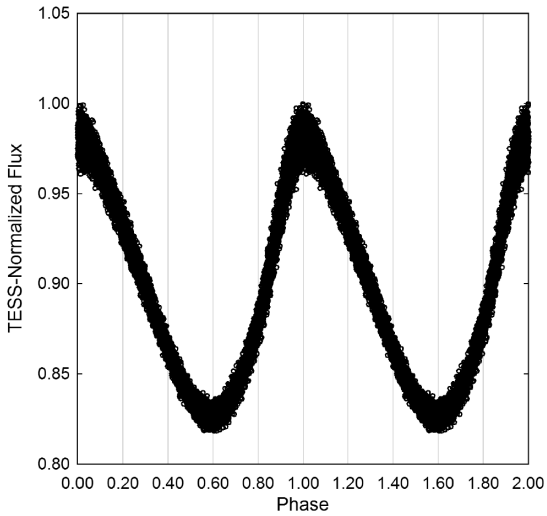

Figure 3. Period-folded (0.0946783 ± 0.0000093 d) LC for V1116 Her produced from peak height normalized photometric data obtained from the TESS satellite between 18 May 2022 and 13 Jun 2022.

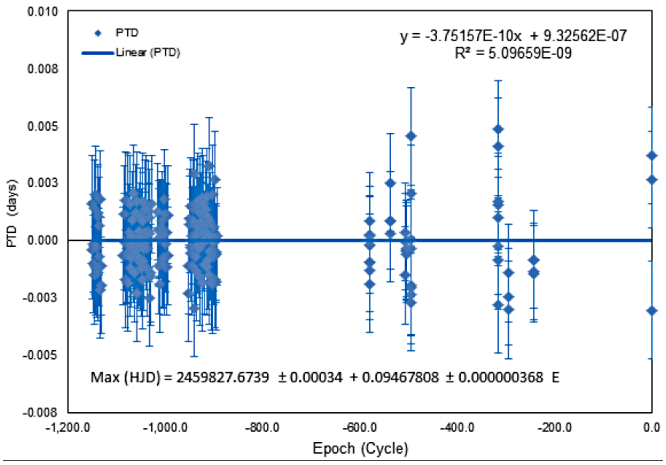

Figure 4. Straight line fit (PTD vs. cycle number) suggesting that little or no change to the fundamental mode pulsation period of V1116 Her had occurred between 1999 and 2018.

Table 3. V1116 Her color indices (B–V) with uncertainty determined at SO along with survey values reported from other sources which were used to estimate $(B–V)_0$[a] and T_{eff}[b].

Source	*(B–V)*	*(B–V) Error*	*$(B–V)_0$[a]*	*$(B–V)_0$ Error*	*log T_{eff}*	*log T_{eff} Error*	*T_{eff}[a]*	*T_{eff} Error*
SO nr max	0.206	0.007	0.159	0.007	3.908	0.003	8093	48
SO nr min	0.277	0.010	0.231	0.010	3.882	0.004	7613	67
SO average	0.242	0.012	0.195	0.012	3.895	0.005	7849	83
APASS[c]	0.291	0.150	0.240	0.150	3.879	0.052	7575	918
2MASS[c]	0.280	0.046	0.234	0.046	3.865	0.014	7320	243
UCAC4[c]	0.362	N/A	0.316	N/A	3.850	N/A	7084	N/A

[a] $(B–V)_0$ = (B–V) – E(B–V) where E(B–V) = 0.0462 ± 0.0008 ((Amôres and Lépine 2005). [b] T_{eff} = effective temperature (K) from Pecaut and Mamajek (2013).[c] Unknown when data acquired during pulsation cycle.

An updated linear ephemeris complete with uncertainties was produced by plotting (Figure 4) the PTD residuals vs. epoch (or cycle number) as follows:

$$\text{Max (HJD)} = 2459827.6739\ (3) + 0.0946781\ (4)\ E. \quad (2)$$

where the times of maxima are in Heliocentric Julian Dates (HJD), and E is an integral cycle number chosen so that E = 0 represents the most recent maximum measurement. A comparison of equations 1 and 2 shows that our data yield a period slightly shorter that the VSX value from August 2020.

B- and V-magnitudes can be combined to produce a (B–V) or color index LC (Figure 5). Care was taken in making this plot to insure that the phase values were the same as those in Figure 2. There is a slight phase shift (~0.05 or about 7 min) between the single-color LCs and the B–V LC. The blue points in Figure 5 were averaged to determine a B–V value near maximum brightness, and the red points were used to find a near-minimum brightness value.

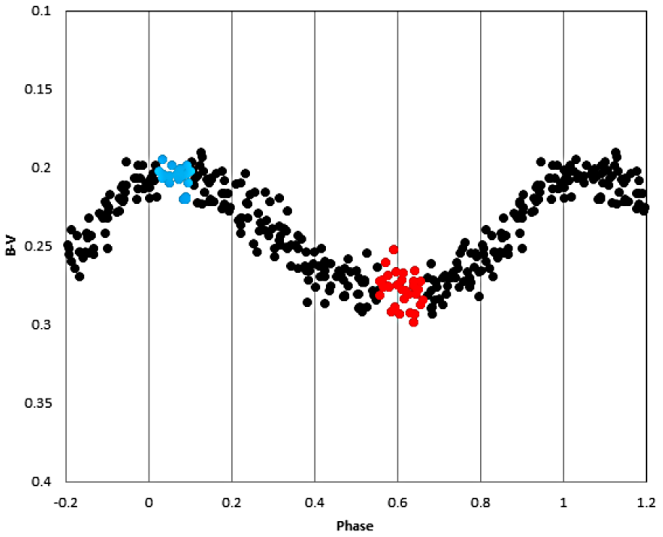

Figure 5. A color excess (B–V) LC for V1116 Her shows significant changes (0.20 < (B–V) < 0.28) as maximum light slowly descends to minimum light. This effect is most closely associated with a decrease in the effective surface temperature during minimum light. Note also the small phase shift (~0.05 or about 7 min) compared to the LCs in Figure 2. The blue points were averaged to determine a B–V value near maximum brightness, and the red points were used to find a near-minimum brightness value.

3.2. Light curve behavior

Light curves from HADS variables are usually asymmetrical with a faster rise from minimum to maximum light and a slower decline back to minimum brightness. V1116 Her appears to be a good example in this regard (Figure 2). The zero phase point in this plot was arbitrarily chosen at maximum brightness. The largest difference between maximum and minimum light is in the B passband (ΔB mag = 0.3443 ± 0.0271), followed by V (ΔV mag = 0.2751 ± 0.0254), R_c (ΔR_c mag = 0.2260 ± 0.0237), and finally I_c (ΔI_c mag = 0.1737 ± 0.0194). This is typical for pulsating F- to A-type stars.

The B–V LC from the SO data shows noticeable reddening (higher B–V value) near minimum light. Averaging a few points near the maximum and minimum of the B–V plot (the blue and red points in Figure 5) yields a quantitative estimate. In this case color excess (B–V) ranges between 0.206 ± 0.007 and 0.277 ± 0.010 mag. Additional color information was found in the APASS, 2MASS, and UCAC4 databases. Both the APASS and UCAC4 listings included B- and V-magnitudes, although no uncertainty was given in the UCAC4 database. The 2MASS information includes only J and K magnitudes with the associated uncertainties so it was necessary to convert these to B and V for comparison. A web site at http://brucegary.net/dummies/method0.html provides equations to convert from J and K to B and V magnitudes. Table 3 lists B–V values from several sources with propagated errors along with $(B–V)_0$ values corrected for interstellar extinction (Amôres and Lépine 2005) and corresponding temperatures, T_{eff} (Pecaut and Mamajek 2013).

The color indices from the surveys are all larger than the average value from the SO data, and either present no uncertainty or have uncertainties that are much larger than the value from the SO data. It is unknown when light curve data from APASS, 2MASS, or UCAC4 were acquired during a pulsation cycle. Before attempting to determine T_{eff} from B–V, it is necessary to consider interstellar extinction, A_V. A value for Galactic (Milky Way) dust reddening or color excess, E(B–V), can be determined from A_V as below:

$$E(B–V) = A_V / 3.1. \quad (3)$$

E(B–V) is commonly used to correct B–V according to:

$$(B–V)_0 = (B–V) – E(B–V). \quad (4)$$

where $(B–V)_0$ is also known as intrinsic color.

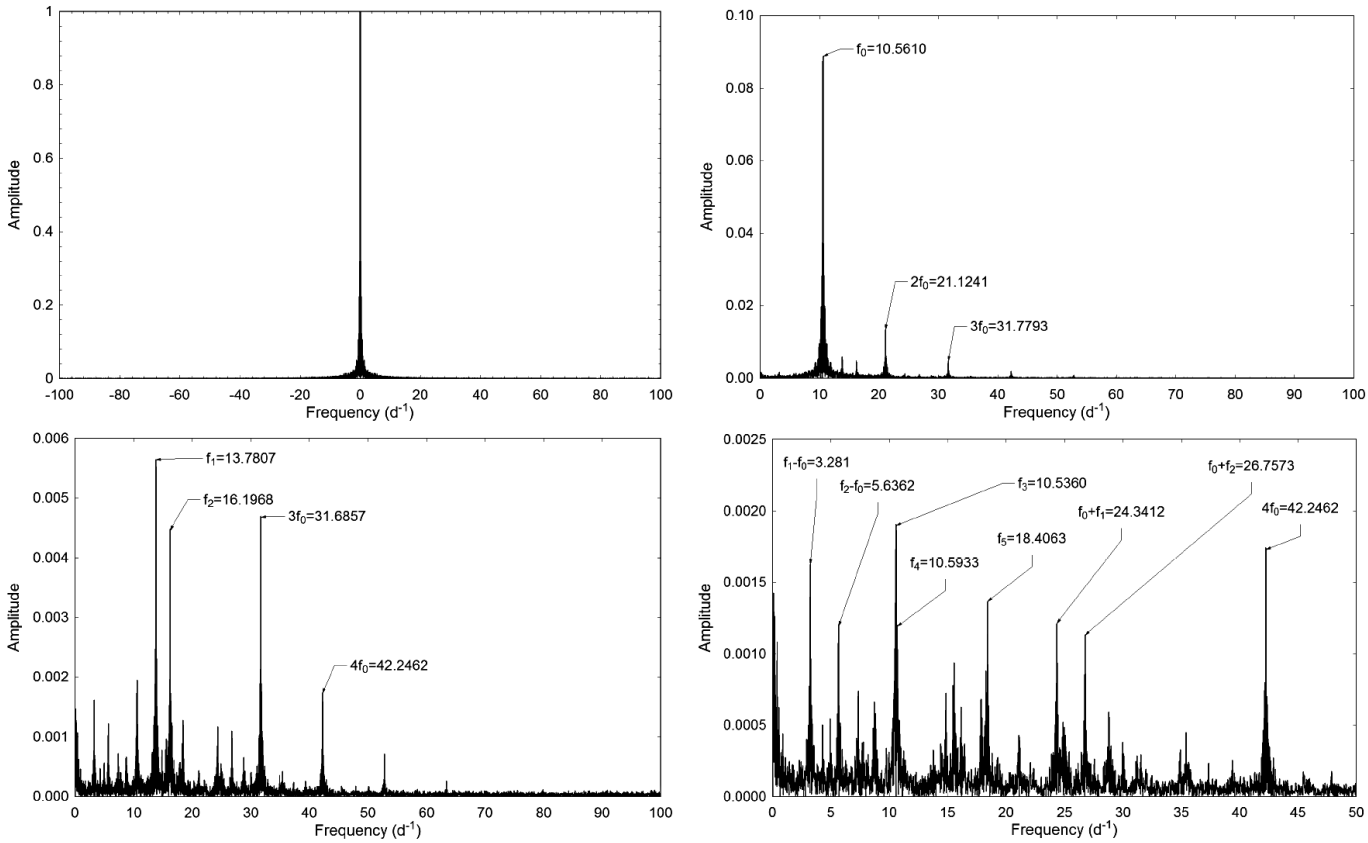

Figure 6. V1116 Her spectrum window and power spectrum plots for all significant frequencies detected (n = 13) from TESS photometry using Discrete Fourier Transformation (Period04).

Estimates for values for E(B–V) can vary depending on the model selected (Amôres and Lépine 2005, 2007; Schlegel *et al.* 1998; Schlafly and Finkbeiner 2011; Schlafly *et al.* 2014). These models can be conveniently accessed via the GALextin website at http://www.galextin.org/ (Amôres *et al.* 2021). For this study, we use the reddening value based on Amôres and Lépine (2005) yielding $A_V = 0.143 \pm 0.003$. From equation 3, $E(B–V) = 0.0462 \pm 0.0008$ mag. From Equation 4, this results in an intrinsic color index $(B–V)_0$ for V1116 Her that varies between 0.159 ± 0.007 at maximum light and 0.231 ± 0.010 mag at minimum brightness, with a mean value of 0.195 ± 0.012. Interpolating these numbers between values from Table 5 in Pecaut and Mamajek (2013) yields a mean effective temperature (T_{eff}) of 7849 ± 83 K, with a minimum T_{eff} of 7613 ± 48 K and a maximum T_{eff} of 8093 ± 48 K. Based solely on B–V photometry at SO, these results compare with the $T_{eff} = 7978^{+373}_{-228}$ K listed in the Gaia DR2. Interestingly, the average B–V from the APASS and 2MASS data yields a value of $T_{eff} = 7450 \pm 470$ K. The SO result corresponds to a spectral class of A7V, while the Gaia DR2 value represents an A6V and the APASS and 2MASS average suggests an A9V. Qian *et al.* (2018) proposed a classification scheme based on a star's T_{eff}. Stars with T_{eff} between 6700 and 8500 K, like V1116 Her, are considered normal δ Scuti (NDST) stars, while cooler ones are classified as unusual and cool variable (UCV) stars.

3.3. Light curve analysis by Discrete Fourier Transformation

Discrete Fourier transformation (DFT) was performed using Period04 (Lenz and Breger 2005). This provided the fundamental mode pulsating frequency (spectral window = 100 d^{-1}).

Table 4. Fundamental frequency ($f_0 = d^{-1}$), corresponding harmonics and combinations detected following DFT analysis of time-series photometric data (TESS) from V1116 Her.

	Freq. (d^{-1})	*Freq. Error**	*Amp. (mag.)*	*Amp. Error**	*Phase*	*Phase Error**	*SNR*
f_0	10.5610	0.0001	0.0728	0.0003	0.8603	0.0007	573.4
$2f_0$	21.1232	0.0001	0.0120	0.0001	0.0120	0.0004	171.8
f_1	13.7807	0.0002	0.0047	0.0001	0.8935	0.0011	49.2
$3f_0$	31.6857	0.0002	0.0043	0.0001	0.5055	0.0012	58.7
f_2	16.1968	0.0002	0.0037	0.0001	0.4487	0.0018	24.7
f_3	10.5360	0.7676	0.0022	0.0001	0.0857	0.2598	17.3
$4f_0$	42.2462	0.0005	0.0016	0.0001	0.4255	0.0041	33.1
$f_1 - f_0$	3.2181	0.0005	0.0015	0.0001	0.2359	0.0033	26.4
$f_0 + f_1$	24.3412	0.0007	0.0012	0.0001	0.7667	0.0049	10.3
f_4	10.5933	0.9934	0.0011	0.0004	0.8033	0.2662	11.4
f_5	18.4063	0.0009	0.0011	0.0001	0.6250	0.0052	11
$f_0 + f_2$	26.7573	0.0512	0.0011	0.0002	0.2684	0.0421	10.7
$f_2 - f_0$	5.6362	0.0007	0.0011	0.0001	0.4879	0.0048	15.6

Successive steps employed pre-whitening to remove the previous most significant signals to look for oscillations within the residuals. This analysis was performed on the BVR_cI_c data from the SO measurements. However, the TESS data are so precise that they produced the most detailed Fourier analysis. According to Baran *et al.* (2015) and Baran and Koen (2021), the detection threshold for frequencies derived from space-based photometry is significantly higher ($S/N \geq 5.4$) than that

Table 5. Global stellar parameters for V1116 Her using values reported from observations at SO and those predicted from evolutionary modelling (PARSEC).

Parameter	*PARSEC*[a]	*PARSEC*[b]	*SO*
Mean T_{eff} [K]	7722±278	7722±278	7722±278
Mass [$M_\odot$]	1.97±0.03	1.55±0.04	2.02±0.04
Radius [$R_\odot$]	2.55±0.09	2.61±0.06	2.60±0.21
Luminosity [$L_\odot$]	21.65±1.74	21.65±1.74	21.65±1.74
rho [g/cm^3]	0.168±0.018	0.123±0.008	0.164±0.041
log g [cgs]	3.92±0.07	3.80±0.02	3.92±0.07
Q [d]	0.032±0.002	0.028±0.001	0.032±0.003
Age [Gyr]	0.934±0.040	1.76±0.01	—

[a] *Bressan* et al. *(2012), Z = 0.020.* [b] *Bressan* et al. *(2012), Z = 0.004.*

typically used for ground-based measurements (S/N ≥ 4). Analysis of the TESS data yielded the 13 frequency components listed in Table 4. Uncertainties in frequency, amplitude, and phase were all estimated using the Monte Carlo simulation (n = 400) routine built into Period04. The column at the left is the authors' assignment of each component as a fundamental mode, f_0, harmonic, nf_0 (n = 1–4), or combination frequency.

The pre-whitening process uncovered two additional oscillation modes, f_3 and f_4, very close to the fundamental mode frequency but with comparatively low amplitudes. Figure 6 includes a spectral window and power spectrum plots for all statistically signficant (n = 13) frequency components revealed by Period04.

Collectively, the results strongly indicate that V1116 Her is not a simple monoperiodic radial pulsator. The presence of at least two other independent oscillations at 13.7807 d^{-1} (f_1) and 16.1968 d^{-1} (f_2) are diagnostic (Stellingwerf 1979) for radial modes at the first ($P_1/P_0 = 0.766$) and second overtones ($P_2/P_0 = 0.652$), where P_0, P_1, and P_2 are the fundamental mode, first overtone, and second overtone periods (d). The spectral window and amplitude spectra derived from the B-, V-, R_c-, and I_c-passbands are not included since they are essentially redundant with respect to the fundamental mode frequency (10.5610 d^{-1}) out to the third harmonic. These ground-based observations did not consistently reveal the first overtone (f_1), and failed to show f_3, f_4, or any of the other independent oscillations beyond $3f_0$. It is unlikely that f_3 and f_4 are rotationally split components of the fundamental mode (f_0), which has been shown to be radial according to the diagnostic calculation ($P_1/P_0 = 0.77$) attributed to Stellingwerf (1979). A more likely explanation is that f_3 and f_4 are low amplitude non-radial modes which are close in frequency to the fundamental radial mode. Additional high resolution spectroscopy designed to establish the rotational velocity of V1116 Her along with high cadence multi-bandpass photometry would prove useful in this regard.

3.4. Global Parameters

Absolute V_{mag} (M_V) was calculated (1.374±0.087) after substituting the Gaia EDR3 distance (907.2±19.1 pc), the observed value for m (V_{avg} = 11.306±0.026), and interstellar reddening (A_V = 0.143±0.003) into the reddening corrected distance modulus:

$$d(pc) = 10^{(m - M_V - A_V + 5)/5)}. \quad (5)$$

The luminosity of V1116 Her in solar units (L_* = 21.65±1.74 $L_\odot$) was calculated according to:

$$L_*/L_\odot = 10^{((M_{bol\odot} - M_{bol*})/2.5)}, \quad (6)$$

where $M_{bol\odot}$ = 4.74 and M_{bol*} = 1.401±0.087. Finally, the radius of V1116 Her in solar units (R_* = 2.60±0.21) was estimated using the well-known relationship where:

$$L_*/L_\odot = (R_*/R_\odot)^2 (T_*/T_\odot)^4. \quad (7)$$

The mass of a single isolated field star is very challenging to determine directly. Nonetheless, according to a model using MS stars in detached binary systems, Eker *et al.* (2018) developed a mass-luminosity relationship ($1.05 < M/M_\odot \leq 2.40$) according to the following equation:

$$\log(L) = 4.329\ (\pm 0.087) \cdot \log(M) + 0.010\ (\pm 0.019). \quad (8)$$

This expression leads to a mass (M_* = 2.046±0.041) in solar units as derived from Equation 7 where L_* = 21.65±1.74 $L_\odot$. All of these values (M_*, R_*, L_*, and T_{eff}) summarized in Table 5 fall well within expectations for a HADS variable. Furthermore, stellar radius was independently estimated from an empirically derived period-radius (P-R) relationship reported by Laney *et al.* (2003) for HADS and classical Cepheids:

$$\log(R_*) = a + b \cdot \log(P) + c, \quad (9)$$

where a = 1.106±0.012, b = 0.725±0.010, and c = 0.029±0.024. In this case the value for R_* (2.47±0.38 $R_\odot$) was somewhat smaller than the value derived from observations at SO (2.60 ±0.21 $R_\odot$).

Results obtained for density ($\rho_\odot$), surface gravity (log g), and pulsation constant (Q) are also included in Table 5. Stellar density (ρ_*) in solar units (g/cm^3) was calculated according to:

$$\rho_* = 3 \cdot M_* \cdot m_\odot / (4\pi (R_* \cdot r_\odot)^3), \quad (10)$$

where $m_\odot$ = solar mass (g), $r_\odot$ = solar radius (cm), M_* is the mass, and R_* the radius of V1116 Her in solar units. Using the same algebraic assignments, surface gravity (log g) was determined by the following expression:

$$\log g = \log (M_* \cdot m_\odot \cdot G) / (R_* \cdot r_\odot)^2). \quad (11)$$

In Equation 11, the gravitational constant G = 6.67408 ×10^8 cm^3 g^{-1} sec^{-2}.

When attempting to characterize p-mode pulsations (radial) it is helpful to introduce the concept of a pulsation constant (Q). The dynamical time that it takes a p-mode acoustic wave to internally traverse a star is related to its size but more accurately the mean density. The mean density of an isolated field star like V1116 Her can not be determined without great difficulty. However, it can be expressed in terms of other measurable stellar parameters where:

$$\log(Q) = -6.545 + \log(P) + 0.5 \log(g) + 0.1 M_{bol} + \log(T_{eff}). \quad (12)$$

The full derivation of this expression is provided in Breger (1990). The resulting Q values (Table 5) derived from observations at SO are consistent with theory (Q = 0.032 d) and the distribution of Q-values (0.03–0.04 d) from fundamental mode radial pulsations observed with other δ Sct variables (Breger 1979; Joshi and Joshi 2015; Antonello and Pastori 1981).

Finally, we attempted to get a relative sense of how the physical size, temperature, and brightness of V1116 Her change over the course of a single 2.27-hour pulsation. As shown in Figure 5 there is a significant increase in reddening (B–V) as maximum light descends to minimum light. Intrinsic color reveals that at maximum light, where $(B–V)_0 = 0.163 \pm 0.035$, the corresponding effective temperature is 7997 ± 79 K, whereas at minimum light ($(B–V)_0 = 0.235 \pm 0.021$) the estimated effective temperature is 7565 ± 76 K. Between these two extremes the putative rise in temperature (+433 K) would correspond to a 1.3-fold increase in luminosity but only a relatively small increase (+0.05 $R_\odot$) in radius. Should radial velocity data become available for this system over an entire oscillation cycle, this rather crude estimate for changes in stellar radius would be best performed using the Baade-Wesselink method developed by Wesselink (1946).

3.5. Evolutionary status of V1116 Her

Now armed with reasonable estimates for luminosity and the effective temperature of V1116 Her, we can attempt to describe the evolutionary status of this variable. These values are plotted in the theoretical Hertzsprung-Russell diagram (HRD) shown in Figure 7. Here, the thick solid line gives the ZAMS position for stars with solar metallicity while two broken lines nearly perpendicular to the ZAMS delimit the blue and red edges of the theoretical instability strip for radial low-p modes (Xiong *et al.* 2016). Asterisks mark the positions of several known HADS, ostensibly both δ Sct and SX Phe types (Balona 2018). The filled circle indicates the position of V1116 Her using the SO derived parameters and corresponding error estimates provided in Table 4. To determine the mass and age of V1116 Her from theoretical evolutionary tracks its metallicity, Z, needs to be known. Unfortunately, this star has not been observed with a high resolution spectrograph so no direct measurement of Z exists, however, we can at least try to estimate its value indirectly. Its distance from the galactic plane (~567 pc) favors a thick disc membership rather than halo. It can therefore be assumed that V1116 Her approaches solar metallicity, or at most a few times lower, which also corresponds to the metallicity of metal-rich globular clusters classified as Oosterhoff type I.

Ironically, a true value for the metallicity of our closest star remains a point of contention. The numbers obtained in the last few decades range between 0.012 and 0.020. Asplund *et al.* (2009) proposed a value where $Z_\odot = 0.0142$. However, von Steiger and Zurbuchen (2016) questioned this result and obtained the value of Z_sun = 0.0196 ± 0.0014 based on the analysis of the chemical composition of the solar wind. Soon thereafter, Serenelli *et al.* (2016) showed that the derived composition is in serious disagreement with observables from the basic solar model so it cannot be representative of the solar interior. Obviously, the problem of a definitive value for $Z_\odot$ still remains an open question. Two different PARSEC evolutionary

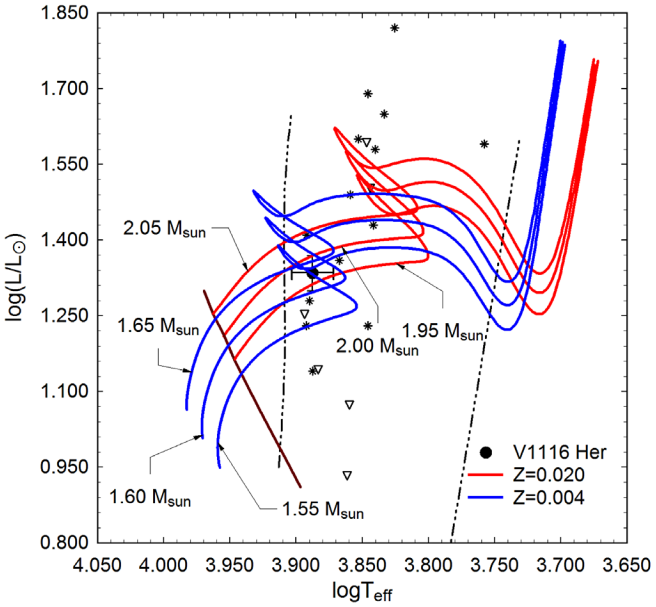

Figure 7. Evolutionary tracks (red solid line: Z = 0.020 and blue solid line: Z = 0.004) derived from PARSEC models (Bressan *et al.* 2012) showing position of V1116 Her (black filled circle) relative to ZAMS (thick maroon line) within the theoretical instability strip (dashed lines) for radial low degree p-mode pulsators. Asterisks denote the positions of known HADS, while open triangles indicate the position of SX Phe pulsators (Balona 2018).

models (Bressan *et al.* 2012) are plotted in Figure 7: the red solid lines show the models when Z = 0.020 and blue solid lines define the models with Z = 0.004. The latter models would correspond to a decrease in metallicity by a factor of 3 to 5 depending on the reference solar metallicity. Opacity (absorption properties in the gas phase) was estimated according to the solar distribution of heavy metals adopted from Caffau and Ludwig (2007) and Caffau *et al.* (2007, 2008a, 2008b, 2009, 2010, 2011) where Z≃0.0152. Assuming Z = 0.020, it can be seen (Figure 7) that V1116 Her has a solar mass of 1.97 ± 0.03, solar radius of 2.55 ± 0.09, and an average age of 0.932 ± 0.040 Gyr. Alternatively, a metal-poor (Z = 0.004) star would likely be slightly larger ($R_\odot = 2.61 \pm 0.06$), less massive ($M_\odot = 1.55 \pm 0.04$), and older (1.76 ± 0.01 Gyr). Under these conditions V1116 Her would fall in the HR diagram region where evolutionary tracks of low metallicity stars zigzag due to a stellar contraction near the end of hydrogen burning in the core. Uncertainty in the determination of mass will hopefully improve in the future should high resolution spectroscopic data become available for the V1116 Her.

4. Conclusions

This first multi-color (BVR_cI_c) CCD study of V1116 Her has produced 206 new times of maximum which lead to an updated linear ephemeris. Potential changes in the pulsation period assessed using the observed and predicted times of maximum suggest that since 1999 no significant change has occurred. Deconvolution of time-series photometric data by discrete Fourier transformation indicates that V1116 Her is a multi-mode radial pulsator dominated by a fundamental mode oscillation ($f_0 \simeq 10.5610\ d^{-1}$) with three other harmonics ($2f_0$–$4f_0$). The existence of two other independent oscillations at 13.7807 d^{-1}

(f_1) and 16.1968 d^{-1} (f_2) are diagnostic (Stellingwerf 1979) for radial modes at the first ($P_1/P_0 = 0.766$) and second overtones ($P_2/P_0 = 0.652$), where P_0, P_1, and P_2 are the fundamental mode, first overtone, and second overtone periods (d). Our adopted T_{eff} (7792 ± 278 K) was consistent with spectral results from the Large Sky Area Multi-Object Fiber Spectroscopic Telescope (LAMOST) survey (Zhao *et al.* 2012) which classified this intrinsic variable as A7V. The fundamental mode pulsation period (0.094682 d), oscillation mode (radial), V_{mag} amplitude (0.275 mag), and LC morphology are all consistent with the defining characteristics of a HADS variable. These criteria alone do not necessarily exclude the possibility that V1116 Her is an example of a field SX Phe-type pulsator. In this case, the estimated mass of V1116 Her (2.01–2.09 $M_\odot$) according to Eker *et al.* (2018) exceeds the generally accepted threshold ($M < 1.3\,M_\odot$) for SX Phe stars (McNamara 2011). Furthermore, evolutionary tracks from the PARSEC model which assume near-solar abundance ($Z = 0.020$) for V1116 Her are best matched by a MS star with a mass of $1.97 \pm 0.03\,M_\odot$ and radius of $2.55 \pm 0.09\,R_\odot$. Given these results, the sum total of evidence points to a HADS rather than an SX Phe variable. Not unexpectedly, Fourier analysis of highly precise light curve data acquired during the TESS satellite mission uncovered pulsation modes not detected from our ground-based observatory.

5. Acknowledgements

Critical data and references related to V1116 Her were identified in the International Variable Star Index (VSX) maintained by the AAVSO. The CDS/VizieR web site (https://vizier.cds.unistra.fr/viz-bin/VizieR) operated at Centre de Données astronomiques de Strasbourg, France proved to be a valuable portal for access to such databases as Gaia DR2, Gaia EDR3, TESS, and other sources. The Gaia DR2 data can be found at http://vizier.cds.unistra.fr/viz-bin/VizieR?-source=I/345/gaia2, and the Gaia EDR3 at http://vizier.cds.unistra.fr/viz-bin/VizieR-2?-source=I%2F350%2Fgaiaedr3&. Publicly-accessible data from LAMOST were also used. The Guoshoujing Telescope (the Large Sky Area Multi-Object Fiber Spectroscopic Telescope LAMOST) is a National Major Scientific Project built by the Chinese Academy of Sciences with funding for the project from the National Development and Reform Commission. LAMOST is operated and managed by the National Astronomical Observatories, Chinese Academy of Sciences. The diligence and dedication shown by all associated with these organizations is very much appreciated.

This work has made use of data from the European Space Agency (ESA) mission Gaia (https://www.cosmos.esa.int/gaia), processed by the Gaia Data Processing and Analysis Consortium (DPAC, https://www.cosmos.esa.int/web/gaia/dpac/consortium). Funding for the DPAC has been provided by national institutions, in particular the institutions participating in the Gaia Multilateral Agreement.

This paper includes data collected by the TESS mission and obtained from the MAST data archive at the Space Telescope Science Institute (STScI). STScI is operated by the Association of Universities for Research in Astronomy, Inc., under NASA contract NAS 5-26555.

We gratefully acknowledge the careful review and helpful commentary provided by the *JAAVSO* referees and editors.

References

Amôres, E. B., and Lépine, J. R. D. 2005, *Astron. J.*, **130**, 659.
Amôres, E. B., and Lépine, J. R. D. 2007, *Astron. J.*, **133**, 1519.
Amôres, E. B., *et al.* 2021, *Mon. Not. Roy. Astron. Soc.*, **508**, 1788.
Antonello, E., and Pastori, L. 1981, *Publ. Astron. Soc. Pacific*, **93**, 237.
Asplund, M., Grevesse, N., Sauval, A. J., and Scott, P. 2009, *Ann. Rev. Astron. Astrophys.*, **47**, 481.
Baade, W. 1956, *Publ. Astron. Soc. Pacific*, **68**, 5.
Baglin, A. 2003, *Adv. Space Res.*, **31**, 345.
Balona, L. A. 2018, *Mon. Not. Roy. Astron. Soc.*, **479**, 183.
Baran, A. S., and Koen, C. 2021, *Acta Astron.*, **71**, 113.
Baran, A. S., Koen, C., and Porkrzywka, B. 2015, *Mon. Not. Roy. Astron. Soc.*, **448**, L16.
Bedding, T. R., *et al.* 2020, *Nature*, **581**, 147.
Berry, R., and Burnell, J. 2005,*The Handbook of Astronomical Image Processing*, 2nd ed., Willmann-Bell, Richmond, VA.
Breger, M. 1979, *Publ. Astron. Soc. Pacific*, **91**, 5.
Breger, M. 1990, *Delta Scuti Newsl.*, **2**, 13.
Breger, M. 2000, *Baltic Astron.*, **9**, 149.
Bressan, A., Marigo, P., Girardi, L., Salasnich, B., Dal Cero, C., Rubele, S., and Nanni, A. 2012, *Mon. Not. Roy. Astron. Soc.*, **427**, 127.
Caffau, E., and Ludwig, H. -G. 2007, *Astron. Astrophys.*, **467**, L11.
Caffau, E., Ludwig, H. -G., Bonifacio, P., Faraggiana, R., Steffen, M., Freytag, B., Kamp, I., and Ayres, T. R. 2010, *Astron. Astrophys.*, **514A**, 92.
Caffau, E., Ludwig, H. -G., Steffen, M., Ayres, T. R., Bonifacio, P., Cayrel, R., Freytag, B., and Plez, B. 2008b, *Astron. Astrophys.*, **488**, 1031.
Caffau, E., Ludwig, H. -G., Steffen, M., Freytag, B., and Bonifacio, P. 2011, *Sol. Phys.*, **268**, 255.
Caffau, E., Maiorca, E., Bonifacio, P., Faraggiana, R., Steffen, M., Ludwig, H. -G., Kamp, I., and Busso, M. 2009, *Astron. Astrophys.*, **498**, 877.
Caffau, E., Sbordone, L., Ludwig, H. -G., Bonifacio, P., Steffen, M., and Behara, N. T. 2008a, *Astron. Astrophys.*, **483**, 591.
Caffau, E., Steffen, M., Sbordone, L., Ludwig, H. -G., and Bonifacio, P. 2007, *Astron. Astrophys.*, **473**, L9.
Chevalier, C. 1971, *Astron. Astrophys.*, **14**, 24.
Cox, J. P. 1963, *Astrophys. J.*, **138**, 487.
Eker, Z., *et al.* 2018, *Mon. Not. Roy. Astron. Soc.*, **479**, 5491.
Gaia Collaboration, *et al.* 2018, *Astron. Astrophys.*, **649A**, 1.
Gilliland, R. L., *et al.* 2010, *Publ. Astron. Soc. Pacific*, **122**, 131.
Guzik, J. A. 2021, *Frontiers Astron. Space Sci.*, **8**, 1.
Henden, A. A., Levine, S. E., Terrell, D., Smith, T. C., and Welch, D. L. 2011, *Bull. Amer. Astron. Soc.*, **43**.
Henden, A. A., Terrell, D., Welch, D., and Smith, T. C. 2010, *Bull. Amer. Astron. Soc.*, **42**, 515.
Henden, A. A., Welch, D. L., Terrell, D., and Levine, S. E. 2009, *Bull. Amer. Astron. Soc.*, **41**, 669.

Hoffmeister, C. 1935, *Astron. Nachr.*, **255**, 401.
Holdsworth, D. L., *et al.* 2014, *Mon. Not. Roy. Astron. Soc.*, **439**, 2078.
ImagesPlus. 2020, ImagesPlus Ver. 6.5 (http://www.mlunsold.com).
Joshi, S., and Joshi, Y. C 2015, *J. Astrophys. Astron.*, **36**, 33.
Kafka, S. 2021, Observations from the AAVSO International Database (https://www.aavso.org/data-download).
Kazarovets, E.V., Samus, N. N., Durlevich, O. V., Kireeva, N. N., and Pastukhova, E. N. 2008, *Inf. Bull. Var. Stars*, No. 5863, 1.
Khruslov, A. V. 2006, *Inf. Bull, Var. Stars*, No. 5699, 1.
Kochanek, C. S., *et al.* 2017, *Publ. Astron. Soc. Pacific*, **129**, 104502.
Laney, C. D., Joner, M., and Rodriguez, E. 2003, in *Interplay of Periodic, Cyclic and Stochastic Variability in Selected Areas of the H-R Diagram*, ed. C. Sterken. Astron. Soc. Pacific Conf. Ser. 292, Astronomical Society of the Pacific, San Francisco, 203.
Leavitt, H. S., and Pickering, E. C. 1912, *Harvard Coll. Obs. Circ.*, **173**, 1.
Lee, Y.-H., Kim, S. S., Shin, J., Lee, J., and Jin, H. 2008, *Publ. Astron. Soc. Japan*, **60**, 551.
Lenz, P., and Breger, M. 2005, *Commun. Asteroseismology*, **146**, 53.
Lindegren, L., *et al.* 2016, *Astron. Astrophys.*, **595A**, 4.
McNamara, D. H. 2000, in *Delta Scuti and Related Stars, Reference Handbook and Proceedings of the 6th Vienna Workshop in Astrophysics*, eds. M. Breger, M. Montgomery, Astron. Soc. Pacific Conf. Ser., 210, Astronomical Society of the Pacific, San Francisco, 373.
McNamara, D. H. 2011, *Astron. J.*, **142**, 110.
Minor Planet Observer. 2010, MPO Software Suite (http://www.minorplanetobserver.com), BDW Publishing, Colorado Springs.
Niu, J.-S., Fu, J.-N., and Zong, W.-K. 2013, *Res. Astron. Astrophys.*, **13**, 1181.
Niu, J.-S., *et al.* 2017, *Mon. Not. Roy. Astron. Soc.*, **467**, 3122.
Paunzen, E., and Vanmunster, T. 2016, *Astron. Nachr.*, **337**, 239.
Pecaut, M. J., and Mamajek, E. E. 2013, *Astrophys. J., Suppl. Ser.*, **208**, 9.
Pojmanski, G. 2002, *Acta Astron.*, **52**, 397.
Poretti, E. 2003a, *Astron. Astrophys.*, **409**, 1031.
Poretti, E. 2003b, in *Interplay of Periodic, Cyclic and Stochastic Variability in Selected Areas of the H-R Diagram*, ed. C. Sterken, ASP Conf. Ser. 292, Astronomical Society of the Pacific, San Francisco, 145.
Poro, A., *et al.* 2021, *Publ. Astron. Soc. Pacific*, **133**, 084201.
Qian, S.-B., Li, L.-J., He, J.-J., Zhang, J., Zhu, L.-Y., and Han, Z.-T. 2018, *Mon. Not. Roy. Astron. Soc.*, **475**, 478.
Ricker, G. R., *et al.* 2015, *J. Astron. Telesc. Instrum. Syst.*, **1**, 014003.
Rodríguez, E., and Breger, M. 2001, *Astron. Astrophys.*, **366**, 178.
Schlafly, E. F., and Finkbeiner, D. P. 2011, *Astrophys. J.*, **737**, 103.
Schlafly, E. F., *et al.* 2014, *Astrophys. J.*, **789**, 15.
Schlegel, D. J., Finkbeiner, D. P., and Davis, M. 1998, *Astrophys. J.*, **500**, 525.
Schwarzenberg-Czerny, A. 1996, *Astrophys. J., Lett.*, **460**, L107.
Serenelli, A., Scott, P., Villante, F. L., Vincent, A. C., Asplund, M., Basu, S., Grevesse, N., and Peña-Garay, C. 2016, *Mon. Not. Roy. Astron. Soc.*, **463**, 2.
Smith, T. C., Henden, A. A., and Starkey, D. R. 2011, in *The Society for Astronomical Sciences 30th Annual Symposium on Telescope Science*, Society for Astronomical Sciences, Rancho Cucamonga, CA, 121.
Software Bisque 2019, TheSky professional edition (https://www.bisque.com).
Stellingwerf, R. F. 1979, *Astrophys. J.*, **227**, 935.
Uytterhoeven K., *et al.* 2011, *Astron. Astrophys.*, **534A**, 125.
von Steiger, R., and Zurbuchen, T. H. 2016, *Astrophys. J.*, **816**, 13.
Walker, G., *et al.* 2003, *Publ. Astron. Soc. Pacific*, **115**, 1023.
Wesselink, W. J. 1946, *Bull. Astron. Inst. Netherlands*, **10**, 91.
Woźniak, P. R., *et al.* 2004, *Astron. J.*, **127**, 2436.
Xiong, D. R., Deng, L., Zhang, C., and Wang, K. 2016, *Mon. Not. Roy. Astron. Soc.*, **457**, 3163.
Yang, T.-Z, Sun, X.-Y., Zuo, Z.-Y., and Liu, H.-W. 2021, *Astron. J.*, **161** 27.
Zhao, G., Zhao, Y.-H., Chu, Y.-Q., Jing, Y.-P., and Deng, L.-C. 2012, *Res. Astron. Astrophys.*, **12**, 723.
Ziaali, E., *et al.* 2019, *Physics of Oscillating Stars*, Banyuls-sur-mer, France (DOI 10.5281/zenodo.1494351).